Materials Science & Engineering A 841 (2022) 143031

Contents lists available at ScienceDirect

Materials Science & Engineering A

journal homepage: www.elsevier.com/locate/msea

# Fatigue performance of stainless tool steel CX processed by laser powder bed fusion

Shahriar Afkhami [a,*], Vahid Javaheri [b], Kalle Lipiäinen [a], Mohsen Amraei [c,d], Edris Dabiri [a], Timo Björk [a]

[a] Laboratory of Steel Structures, LUT University, Lappeenranta, 53850, Finland
[b] Materials and Mechanical Engineering, University of Oulu, 90014, Finland
[c] Laboratory of Laser Materials Processing and Additive Manufacturing, LUT University, Lappeenranta, 53850, Finland
[d] Department of Mechanical and Materials Engineering, University of Turku, Turku, 20520, Finland

ARTICLE INFO

*Keywords:*
Additive manufacturing
Laser powder bed fusion
CX
Fatigue
Fractography

ABSTRACT

This study investigates the fatigue performance of additively manufactured steel CX under uniaxial high cycle loading. The results show that surface quality was the most influential parameter that changed the fatigue behavior of the material, compared to combinations of building orientation and heat treatment as other fabrication parameters. Consequently, improving the surface quality from Ra = 3 μm–1 μm increased the fatigue limit from 170 MPa to 250 MPa. However, heat treatment did not significantly influence the fatigue performance of the material, although it increased the hardness of the material from 320 HV to 460 HV.

## 1. Introduction

Stainless tool steel CX (13Cr10Ni1.7Mo2Al0.4Mn0.4Si), as a newly developed precipitation hardening metal for additive manufacturing, has shown great potential to replace typically additively manufactured maraging steels and some other more expensive high-strength alternatives, e.g., titanium-based alloys. This potential is due to the high strength, relatively good thermal stability, and significant corrosion resistance of CX steel. In addition, the strength of this steel can be significantly enhanced by aging treatment due to the precipitation of superlattice (ultrafine) structures made of coherent β-NiAl particles [1–3]. This steel powder has recently been developed by EOS GmbH to be used as a raw powder for the laser powder bed fusion (L-PBF) process. However, many physical and mechanical properties of additively manufactured CX have not been comprehensively identified and require further research. The lack of data can be attributed to the fact that the material has only recently become commercially available, and most studies on CX processed with L-PBF (L- PBF CX) have so far focused on its microstructure or quasi-static mechanical properties. This lack of knowledge is further prominent concerning the fatigue performance of L-PBF CX.

As regards, Ćirić-Kostić et al. [4] investigated the mechanical behavior of L-PBF CX under rotational bending loads. In addition, the effects of machining and shot-peening on the fatigue performance of the material were included in Ref. [4]. However, the fatigue performance of the material with raw surface quality and the effect of building orientation were not considered in Ref. [4]. Therefore, although there have been numerous studies dedicated to the mechanical performance of martensitic metals and steels [5–9], the literature still lacks data on the mechanical performance of L-PBF CX under standard uniaxial fatigue tests and the fatigue performance of L-PBF CX in its as-built condition or with the raw surface quality. Furthermore, the influence of heat treatment, surface quality, and building direction of L-PBF CX on its response to uniaxial cyclic loads has not been investigated. Thus, this study aimed to fill these knowledge gaps and contribute to the available data on L-PBF CX. It should be noted that the microstructural features of L-PBF CX, its hardness, notch toughness, strain hardening behavior, and quasi-static mechanical properties are comprehensively investigated and discussed in a prior study [1]; Therefore, the present research is a step further towards completing the technical knowledge about L-PBF CX.

## 2. Materials and methods

Fresh gas atomized CX powder (13Cr10Ni1.7Mo2Al0.4Mn0.4Si) from EOS GmbH with a particle size distribution of 20–65 μm was used

* Corresponding author.
*E-mail address:* Shahriar.Afkhami@lut.fi (S. Afkhami).

https://doi.org/10.1016/j.msea.2022.143031
Received 24 January 2022; Received in revised form 9 March 2022; Accepted 22 March 2022
Available online 24 March 2022

to manufacture the samples with an EOS M290 system [10]. Samples were manufactured for the high cycle fatigue (HCF) test using the dimensions shown in Fig. 1 per ASTM E466 [11]. The HCF tests were performed at room temperature (≈20 °C) using a 100 kN force-controlled test rig equipped with a 50 kN load cell. The loading ratio ($R$) and frequency of the tests were 0.1 and 3 Hz, respectively. In order to investigate the synergistic effects of building direction, surface quality, and heat treatment, the samples were divided into five sets following their fabrication procedures, as shown in Table 1. Machined specimens were subjected to 500 μm of material removal, and heat-treated specimens were subjected to annealing at 850 °C for 30 min and subsequent aging at 525 °C for 120 min. Further detail on the fabrication approach and procedures can be found in Ref. [1]. After HCF tests, the fracture surfaces of the samples were examined using a Hitachi SU3500 scanning electron microscope (SEM) equipped with an energy-dispersive X-ray spectroscopy (EDS) probe. Finally, the surface roughness (quality) and Vickers hardness of the specimens were measured using a KEYENCE VE-3200 3D microscope and Struers DuraScan 70 (by applying 3 Kgf for 10 s), respectively. Reported hardness values are the average of five consecutive measurements in each case.

## 3. Results and discussion

The stress amplitude-fatigue life (S–N) data of L-PBF CX are presented in Fig. 2. According to the results, L-PBF CX with raw surface had the most inferior fatigue performance, with or without being heat-treated. Therefore, the heat treatment did not improve the fatigue life of the material with the raw surface, and the surface quality had the dominant role in determining the fatigue performance of the material. On the other hand, mechanical machining increased the fatigue limit by ≈ 50%, regardless of the building direction and heat treatment condition, by improving the average surface quality from $Ra$[1] = 3 μm and $Rz$[2] = 20 μm to $Ra$ = 1 μm and $Rz$ = 5 μm. In other words, although the heat treatment and horizontal building direction significantly improved the material strength under quasi-static unidirectional tensile loads [1], their combination had a negligible influence on the fatigue performance of the material in the HCF test. This phenomenon has also been observed in 18Ni300 as another additively manufactured maraging steel [12–14].

According to the literature, the increase in the hardness and strength of these steels after heat treating them make these materials more defect sensitive and can even reduce their fatigue life [12,13]. The fatigue limits of high strength steels under fully reversed loadings ($\sigma_{f(R=-1.0)}$) are traditionally expected to be 30% of their ultimate tensile strengths ($\sigma_{UTS}$) [14]. By using the modified Goodman equation (Eq. (1)) [15] to convert fatigue limits from HCF tests in this study ($\sigma_{f(R=0.1)}$) to $\sigma_{f(R=-1.0)}$, the fatigue performances of different specimen sets are compared in Table 2.

$$[\sigma_{f(R=0.1)} / \sigma_{f(R=-1.0)}] + [(\text{mean stress for } R = 0.1) / \sigma_{UTS}] = 1. \quad (1)$$

The comparisons from Table 2 point to the significant role of surface defects in the fatigue failure of L-PBF CX and its high defect sensitivity even in its as-built condition since only the VM specimens, with their surface defects removed by machining, followed the traditional behavior of high strength steels (having the lowest error of ≈6% among all the sets). It should be noted that horizontal samples in their as-built condition are expected to have a slightly higher fatigue limit than the VA and VM specimens since $\sigma_{UTS}$ of the horizontal specimens in Ref. [1] were ≈7% higher than those of their vertical peers; however, horizontal as-built samples had to be excluded from the current study due to the limited number of specimens. Consequently, only horizontal heat-treated samples are investigated here.

Furthermore, the fractography of the samples clarified the dominant role of surface defects in the fatigue performance of L-PBF CX further. As shown in Fig. 3, the failure of the samples with raw surface quality (VA and HTVA) was triggered by their surface defects, whether the material was heat treated or as-built. However, the machined samples (VM and

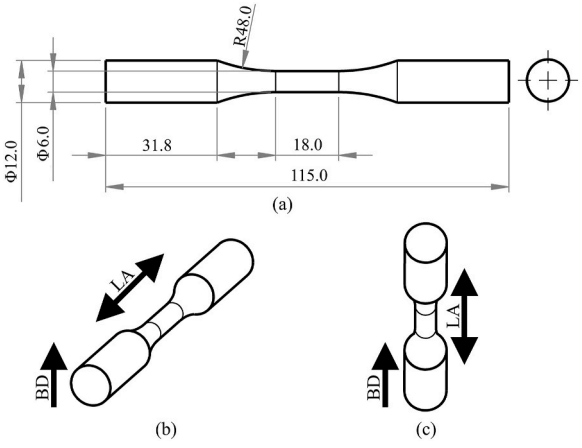


**Fig. 1.** The dimensions (in mm) of the fatigue samples are shown in (a). The alignments of the loading axis (LA) and building direction (BD) are shown in (b) for horizontal and (c) for vertical samples.

[1] Average roughness.
[2] Maximum roughness depth.

**Table 1**
Sample sets and their specifications.

| Sample code | building direction | surface quality | heat treatment condition |
|---|---|---|---|
| **VA** | vertical | raw | As-built |
| **VM** | vertical | machined | As-built |
| **HTVA** | vertical | raw | Heat-treated |
| **HTVM** | vertical | machined | Heat-treated |
| **HTHM** | horizontal | machined | Heat-treated |

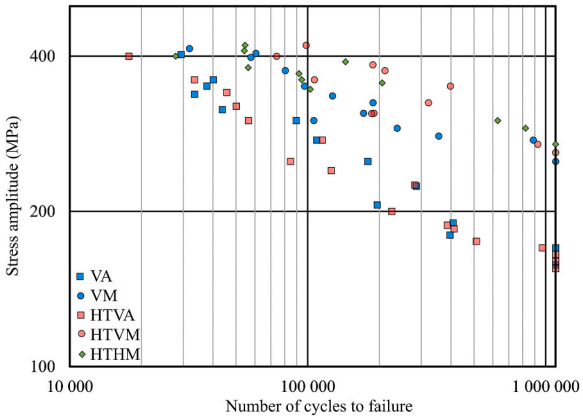


**Fig. 2.** S–N data of L-PBF CX according to its fabrication procedure.

**Table 2**
Estimated fatigue limits of L-PBF CX and their comparisons.

| Sample code | $\sigma_{f(R=0.1)}$ | $\sigma_{f(R=-1.0)}$ | 30% of $\sigma_{UTS}$ [1] | Error[a] |
|---|---|---|---|---|
| **VA** | 170 MPa | 211 MPa | 324 MPa | −54% |
| **VM** | 250 MPa | 348 MPa | 327 MPa | +6% |
| **HTVA** | 165 MPa | 188 MPa | 493 MPa | −162% |
| **HTVM** | 260 MPa | 321 MPa | 505 MPa | −58% |
| **HTHM** | 270 MPa | 336 MPa | 504 MPa | −50% |

[a] Error (%) = $[(\sigma_{f(R=-1.0)} - (30\% \text{ of } \sigma_{UTS}))/\sigma_{f(R=-1.0)}] \times 100$.

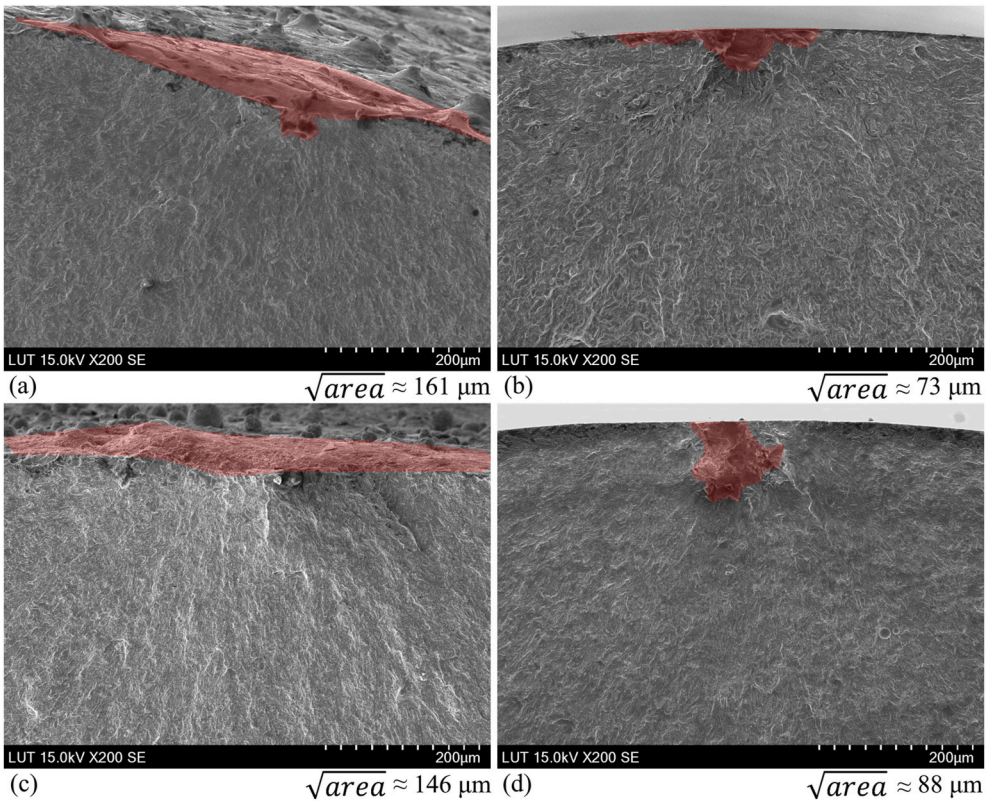


**Fig. 3.** Critical defects (highlighted red areas) of the (a) VA sample fractured under the lowest stress amplitude, (b) VM sample fractured under the lowest stress amplitude, (c) HTVA sample fractured under the lowest stress amplitude, and (d) HTVM sample fractured under the lowest stress amplitude. (For interpretation of the references to colour in this figure legend, the reader is referred to the Web version of this article.)

HTVM) failed from smaller subsurface defects compared to specimens with raw surface quality. According to the EDS analysis (Fig. 4), these subsurface defects were chromium- or aluminum-reach intermetallic compounds. In addition, comparisons of Fig. 3(a) with Fig. 3(c) and (b) with Fig. 3(d) show that the heat treatment did not significantly change the size of the critical defects from which the fatigue fractures originated.

The average hardness of L-PBF CX was measured as 320 HV and 460 HV in its as-built and heat-treated conditions, respectively. Further, the Murakami approach can be used to investigate the correlation between the fatigue life of steels with Vickers hardness values lower than 400 HV [15]. Consequently, the Murakami approach was used to estimate the fatigue life of L-PBF CX in its as-built condition using the critical defects detected in Fig. 3(a) and (b). The results of the fatigue life estimations using Murakami equations for failures from surface and subsurface defects (Eq. (2) and Eq. (3), respectively [16]) are summarized in Table 3.

$$\sigma_{f(R=0.1)} = [1.43(HV + 120) / (\sqrt{area})^{(1/6)}] \times [(1 - R) / 2]^{(0.226+0.0001HV)}, \quad (2)$$

$$\sigma_{f(R=0.1)} = [1.41(HV + 120) / (\sqrt{area})^{(1/6)}] \times [(1 - R) / 2]^{(0.226+0.0001HV)}. \quad (3)$$

**Table 3**
Fatigue life values according to the HCF tests and Murakami approach.

| Sample code | Experimental $\sigma_{f(R=0.1)}$ | Estimated $\sigma_{f(R=0.1)}$ | Error[a] |
|---|---|---|---|
| **VA** | 170 MPa | 220 MPa | −29% |
| **VM** | 250 MPa | 247 MPa | +2% |

[a] Error (%) = [(experimental $\sigma_{f(R=0.1)}$ - estimated $\sigma_{f(R=0.1)}$)/experimental $\sigma_{f(R=0.1)}$] × 100.

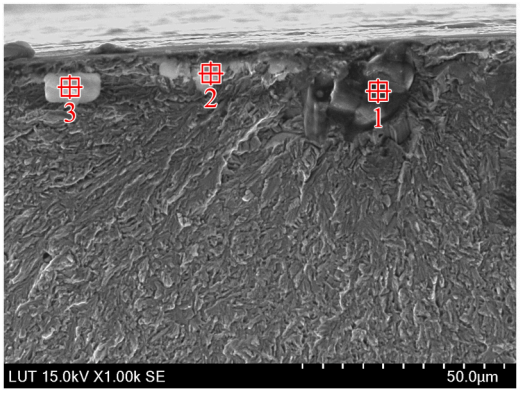


| Point 1 | | | | | | |
|---|---|---|---|---|---|---|
| Element | O | Al | Ca | Cr | Ni | Fe |
| wt% | 30.80 | 62.14 | – | 3.36 | – | Bal. |

| Point 2 | | | | | | |
|---|---|---|---|---|---|---|
| Element | O | Al | Ca | Cr | Ni | Fe |
| wt% | 15.65 | 2.03 | 3.46 | 10.58 | – | Bal. |

| Point 3 | | | | | | |
|---|---|---|---|---|---|---|
| Element | O | Al | Ca | Cr | Ni | Fe |
| wt% | 9.63 | 2.35 | 1.37 | 11.34 | 6.56 | Bal. |

**Fig. 4.** EDS analysis of the subsurface defects discovered from the fracture surface of an HTHM specimen failed under the maximum stress of 911 MPa.

Accordingly, similar to the conclusion from Table 2, the fatigue limit of the as-built samples with machined surface quality mostly agreed with the theoretical estimations. However, it should be noted that, instead of being failed from individual surface flaws, the VA specimens can be considered failed from an array of (interconnected) surface defects stemming from valleys and protrusions (features related to their rough surface). This assumption agrees with the fractography images taken in lower magnifications, as shown in Fig. 5 as an example. In such a case, Murakami suggested considering the $\sqrt{\text{area}}$ of overall defects equal to $d\sqrt{10}$ ($d$ being the most critical depth related to surface defects) [15]. Following the visual data from Fig. 5, $d$ can be estimated to be 100 μm for the VA specimens. Consequently, the estimated $\sigma_{f(R=0.1)}$ for the VA samples can be calculated as 196 MPa by simultaneously using Eq. (2) and the correction factor. However, although the estimation error was reduced from −29% to −15% using Murakami's correction factor, the error is still significantly higher than the results of the VM specimens (2% error).

## 4. Conclusions

The mechanical performance of L-PBF CX under cyclic loads has been examined via high cycle fatigue tests. The results showed the surface roughness as the most determining parameter regarding the fatigue life of the material. Based on the results, these points can be drawn as the conclusions of this study:

- The synergistic effects of the heat treatment and building direction on the fatigue performance were negligible compared to the surface quality. In other words, although the heat treatment increased the hardness from 320 HV to 460 HV, it did not significantly increase the fatigue limit of the material. However, decreasing the surface roughness from Ra = 3 μm to Ra = 1 μm improved the fatigue limit of the material from 170 MPa to 250 MPa.
- Samples with machined surfaces (highest surface quality) best fitted the theoretical estimations. In other words, the response of machined L-PBF CX to cyclic loads was the closest to the response of conventional high strength steels.

Finally, although the thorough understanding of the behavior of L-PBF CX and the discovery of other parameters that influence the fatigue performance of this material requires further research, the initial results of this study show the promising performance of L- PBF CX under cyclic loading. Furthermore, this study proposes improving the surface quality as the most effective approach towards increasing the fatigue life of L-PBF CX. In this regard, investigating the effects of alternative surface treatments, e.g., high-frequency mechanical impact processing and some other approaches associated with surface plastic deformations [17–19], is encouraged for future research.

## Data availability statement

The raw/processed data required to reproduce these findings can be obtained upon request from the corresponding author.

## Originality statement

I write on behalf of myself and all co-authors to confirm that the results reported in the manuscript are original and neither the entire work, nor any of its parts have been previously published. The authors confirm that the article has not been submitted to peer review, nor has been accepted for publishing in another journal. The author(s) confirms that the research in their work is original, and that all the data given in the article are real and authentic. If necessary, the article can be recalled, and errors corrected.

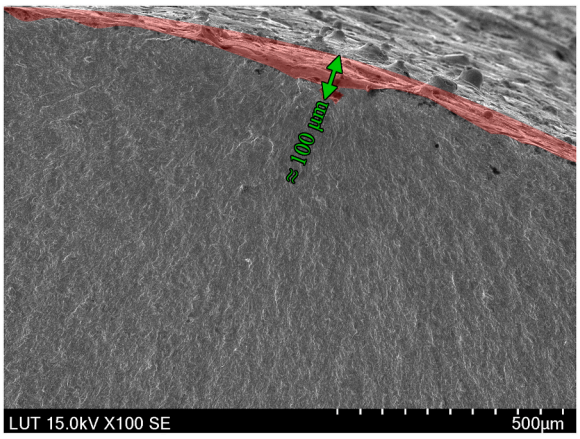


**Fig. 5.** Fractography image of the VA specimen from Fig. 3(a) under lower magnification.

## CRediT authorship contribution statement

**Shahriar Afkhami:** Conceptualization, Methodology, Software, Investigation, Writing – original draft, Writing – review & editing, Visualization. **Vahid Javaheri:** Conceptualization, Methodology, Investigation, Validation, Writing – review & editing. **Kalle Lipiäinen:** Conceptualization, Methodology, Investigation, Validation, Writing – review & editing. **Mohsen Amraei:** Methodology, Validation, Writing – review & editing. **Edris Dabiri:** Conceptualization, Methodology, Validation, Writing – original draft, Writing – review & editing. **Timo Björk:** Conceptualization, Writing – review & editing, Supervision, Funding acquisition.

## Declaration of competing interest

The authors declare that they have no known competing financial interests or personal relationships that could have appeared to influence the work reported in this paper.

## Acknowledgments

This study was conducted at LUT University as a part of the project "Verkostoitumisella voimaa 3D-tulostukseen (VERKOTA, project code: A76589)" funded by the European Regional Development Fund (ERDF).

## References

[1] S. Afkhami, V. Javaheri, E. Dabiri, H. Piili, T. Björk, Effects of manufacturing parameters, heat treatment, and machining on the physical and mechanical properties of 13Cr10Ni1·7Mo2Al0·4Mn0·4Si steel processed by laser powder bed fusion, Mater. Sci. Eng., A 832 (2022) 142402, https://doi.org/10.1016/j.msea.2021.142402.
[2] A. Shahriari, L. Khaksar, A. Nasiri, A. Hadadzadeh, B.S. Amirkhiz, M. Mohammadi, Microstructure and corrosion behavior of a novel additively manufactured maraging stainless steel, Electrochim. Acta 339 (2020) 135925, https://doi.org/10.1016/j.electacta.2020.135925.
[3] A. Hadadzadeh, A. Shahriari, B.S. Amirkhiz, J. Li, M. Mohammadi, Additive manufacturing of an Fe–Cr–Ni–Al maraging stainless steel: microstructure evolution, heat treatment, and strengthening mechanisms, Mater. Sci. Eng. 787 (2020) 139470, https://doi.org/10.1016/j.msea.2020.139470.
[4] S. Ćirić-Kostić, D. Croccolo, M. de Agostinis, S. Fini, G. Olmi, L. Paiardini, F. Robusto, Z. Šoškić, N. Bogojević, Fatigue response of additively manufactured Maraging Stainless Steel CX and effects of heat treatment and surface finishing, Fatig. Fract. Eng. Mater. Struct. (2021), https://doi.org/10.1111/ffe.13611.
[5] S. Afkhami, H. Piili, A. Salminen, T. Björk, Effective parameters on the fatigue life of metals processed by powder bed fusion technique: a short review, Procedia Manuf. 36 (2019) 3–10, https://doi.org/10.1016/j.promfg.2019.08.002.
[6] S. Afkhami, M. Dabiri, S.H. Alavi, T. Björk, A. Salminen, S. Habib Alavi, T. Björk, A. Salminen, Fatigue characteristics of steels manufactured by selective laser melting, Int. J. Fatig. 122 (2019) 72–83, https://doi.org/10.1016/j.ijfatigue.2018.12.029.

[7] J.-T. Fan, Y.-M. Yan, Gradient microstructure with martensitic transformation for developing a large-size metallic alloy with enhanced mechanical properties, Mater. Des. 143 (2018) 20–26, https://doi.org/10.1016/j.matdes.2018.01.055.
[8] J. Fan, L. Zhu, J. Lu, T. Fu, A. Chen, Theory of designing the gradient microstructured metals for overcoming strength-ductility trade-off, Scripta Mater. 184 (2020) 41–45, https://doi.org/10.1016/j.scriptamat.2020.03.045.
[9] J. Fan, M. Jiang, Strain hardenability of a gradient metallic alloy under high-strain-rate compressive loading, Mater. Des. 170 (2019) 107695, https://doi.org/10.1016/j.matdes.2019.107695.
[10] EOS, Materials for Metal Additive Manufacturing, 2019. https://www.eos.info/material-m. (Accessed 10 October 2019).
[11] ASTM, ASTM E466 - 15, Standard Practice for Conducting Force Controlled Constant Amplitude Axial Fatigue Tests of Metallic Materials, ASTM International, 2015, https://doi.org/10.1520/E0466-15.
[12] G. Meneghetti, D. Rigon, D. Cozzi, W. Waldhauser, M. Dabalà, Influence of build orientation on static and axial fatigue properties of maraging steel specimens produced by additive manufacturing, Procedia Struct. Integr. 7 (2017) 149–157. https://www.sciencedirect.com/science/article/pii/S2452321617304262. (Accessed 7 November 2018).
[13] G. Meneghetti, D. Rigon, C. Gennari, An analysis of defects influence on axial fatigue strength of maraging steel specimens produced by additive manufacturing, Int. J. Fatig. 118 (2019) 54–64. https://www.sciencedirect.com/science/article/pii/S0142112318304468. (Accessed 7 November 2018).
[14] C. Elangeswaran, K. Gurung, R. Koch, A. Cutolo, B. van Hooreweder, Post-treatment selection for tailored fatigue performance of 18Ni300 maraging steel manufactured by laser powder bed fusion, Fatig. Fract. Eng. Mater. Struct. 43 (2020) 2359–2375, https://doi.org/10.1111/ffe.13304.
[15] S. Afkhami, E. Dabiri, K. Lipiäinen, H. Piili, T. Björk, Effects of notch-load interactions on the mechanical performance of 3D printed tool steel 18Ni300, Addit. Manuf. 47 (2021) 102260, https://doi.org/10.1016/J.ADDMA.2021.102260.
[16] Y. Murakami, H. Masuo, Y. Tanaka, M. Nakatani, Defect analysis for additively manufactured materials in fatigue from the viewpoint of quality control and statistics of extremes, in: Procedia Structural Integrity, Elsevier B.V., 2019, pp. 113–122, https://doi.org/10.1016/j.prostr.2019.12.014.
[17] S. Afkhami, M. Dabiri, H. Piili, T. Björk, Effects of manufacturing parameters and mechanical post-processing on stainless steel 316L processed by laser powder bed fusion, Mater. Sci. Eng., A 802 (2021) 140660, https://doi.org/10.1016/j.msea.2020.140660.
[18] J. Fan, T. Fu, Toughened austenitic stainless steel by surface severe plastic deformation, Mater. Sci. Eng. A 552 (2012) 359–363, https://doi.org/10.1016/j.msea.2012.05.052.
[19] J.T. Fan, A.Y. Chen, M.W. Fu, J. Lu, A novel structural gradient metallic glass composite with enhanced mechanical properties, Scripta Mater. 61 (2009) 608–611, https://doi.org/10.1016/j.scriptamat.2009.05.046.